Influence of lossless and lossy, heterogeneous environments on Ground Penetrating Radar antenna behaviour

Craig Warren and Antonios Giannopoulos
Institute for Infrastructure and Environment
School of Engineering
The University of Edinburgh
Edinburgh, Scotland, UK
Craig.Warren@ed.ac.uk, A.Giannopoulos@ed.ac.uk

***Abstract*—Directly measuring the radiation characteristics of Ground Penetrating Radar (GPR) antennas in complex environments, typically encountered in GPR surveys, presents many practical difficulties. However it is crucial to be able to understand how energy is being transmitted and received by the antenna. This in turn is important for areas of research such as GPR antenna design, GPR system design, and data processing and inversion algorithms. To overcome these practical challenges an advanced modelling toolset has been developed. It enables detailed 3D Finite-Difference Time-Domain (FDTD) models of GPR antennas to be used in realistic environments that include models of heterogeneous soils. A semi-empirical soil model was utilised, which relates the relative permittivity of the soil to the bulk density, sand particle density, sand fraction, clay fraction and water volumetric fraction. In this initial investigation clear differences in the directivity (power and pattern shape) of the antenna have been observed between a lossless dielectric environment and a more realistic environment featuring a heterogeneous soil model. These findings are part of an on-going parametric study incorporating a range of different soils, soil property distributions, and the inclusion of rough surface modelling.**

I. Introduction

The diversity of Ground Penetrating Radar (GPR) usage means there are a variety of different GPR systems and antennas. Understanding how energy is transmitted and received by a particular GPR antenna has many benefits: improved antenna design, enhanced data processing and inversion algorithms, better informed usage of the antenna in GPR surveys, and improved interpretation of GPR responses. The radiation characteristics of any antenna are usually investigated by analysing parameters such as impedance, field pattern shape, and directivity in free space. This is no different for GPR antennas, but crucially these characteristics must be studied be in the different environments that can be encountered in GPR surveys. This is because a complex series of interactions occur between the antenna and the environment, which change how the antenna behaves.

Radiation pattern measurements in free space of simple antennas, as well as for more widely-used commercial GPR antennas, have been made [1]–[3]. There have also been laboratory measurements of radiation patterns of simple antennas over homogeneous materials obtained directly with another antenna [4], and indirectly through the recording of responses from a simple target [3], [5]. Received energy patterns were measured from a commercial GPR antenna in a series of oil-in-water emulsions which represented lossy homogeneous environments [6]. However, measuring antenna radiation patterns in lossy, heterogeneous environments that are realistic for GPR, presents many practical difficulties. This has prompted researchers to develop numerical simulations of GPR antenna radiation patterns.

Simple and more complex antennas have been modelled in free space, and simple antennas have been modelled in realistic environments, but there have been very limited studies that combine realistic GPR antenna models with realistic environments. Models of antennas over layered media have been developed for an off-ground horn antenna using linear transfer functions [7] and for an antenna operating in the near-field using equivalent sets of infinitesimal electric dipoles [8]. The energy distribution of a shielded dipole antenna over various lossless half-spaces was studied by [9], and similarly [6] used an FDTD antenna model to compare simulated and measured data.

This paper presents an investigation of the radiation characteristics a high-frequency GPR antenna in lossless homogeneous and lossy, heterogeneous environments using detailed FDTD models. An advanced simulation toolset has been developed that allowed a detailed model of a GPR antenna to be used in heterogeneous environments that simulate realistic soils. The first part of the paper focuses on describing the FDTD model and its development. In the second part of the paper results from the simulations are presented. Principal electric and magnetic field plane patterns are compared for lossless dielectrics and lossy, heterogeneous environments.

II. Finite-Difference Time-Domain models

All of the simulations conducted for this research used gprMax (http://www.gprmax.com) which is an electromagnetic wave simulator based on the FDTD method. gprMax was

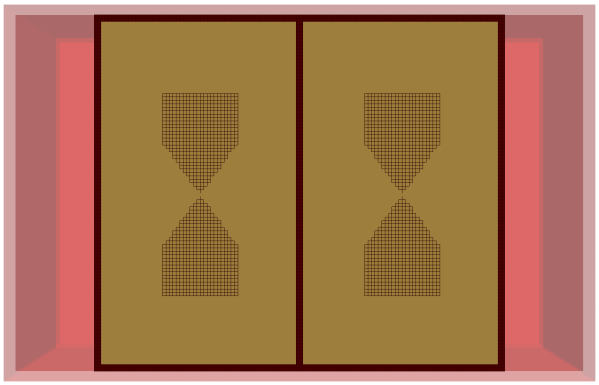

Fig. 1. View of the FDTD mesh of antenna model (skid removed)

originally developed in 1996 [10] and over the past 19 years has been one of the most widely used simulation tools in the GPR community. It has been successfully used for a diverse range of applications in academia and industry [11]–[14], and has been cited nearly 200 times since 2005 [15]. gprMax has recently undergone significant modernisations to the code and also added a number of new advanced features including: an unsplit implementation of higher order perfectly matched layers (PMLs) using a recursive integration approach; uniaxially anisotropic materials; dispersive media using multiple Debye, Drude or Lorenz expressions; improved soil modelling using a semi-empirical formulation for dielectric properties and fractals for geometric characteristics; rough surface generation; and the ability to embed complex transducers and targets.

A. Antenna model

The simulations included a model of the antenna that is representative of a Geophysical Survey Systems, Inc. (GSSI) 1.5 GHz antenna. The antenna model includes all of the main features and geometry of the real antenna. Details of the antenna model development and initial validation can be found in [16]. Fig. 1 shows a view of the detailed FDTD mesh of the geometry of the antenna. A spatial discretisation of $\Delta x = \Delta y = \Delta z = 1$ mm was chosen as a good compromise between accuracy and computational requirements. The Courant Friedrichs Lewy (CFL) condition was enforced which resulted in a time-step of Δt = 1.926 ps.

B. Lossy, heterogeneous soil models

gprMax was used to build lossy, heterogeneous environments that represent soils with more realistic dielectric and geometrical properties. A semi-empirical model, initially suggested by [17], is used to describe the dielectric properties of the soil. The model relates the relative permittivity of the soil to bulk density, sand particle density, sand fraction, clay fraction and water volumetric fraction. Using this approach, a more realistic soil with a stochastic distribution of the aforementioned parameters can be modelled. The real and imaginary parts of this semi-empirical model can be approximated using a multi-pole Debye function plus a conductive term. This dispersive behaviour has been implemented in gprMax by using a recursive convolution method to express dispersive properties as apparent current density sources [18]. Fig. 2 shows the antenna model on a heterogeneous soil model with realistic dielectric and geometrical properties.

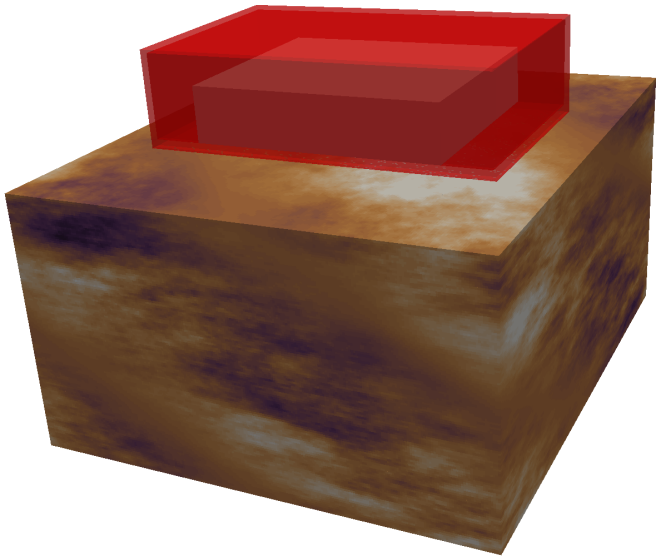

Fig. 2. Antenna model on a heterogeneous soil model with a stochastic distribution of the volumetric water fraction.

III. Modelled radiation patterns

Traditionally antenna patterns are plotted at a specific single frequency, however this is of limited use in analysing the overall performance of an ultra-wideband (UWB) GPR antenna. Instead measures of the total energy given by Eq. (1), adapted from [9], were used.

$$E_{tot}(r,\theta) = \sum_{t}^{T} E(r,\theta)^2 \quad (1)$$

E_{tot} is the total energy at a specific radius (r) and angle (θ); the summation is made over the duration of the time-domain response; and E is the electric field value at a given radius (r) and angle (θ). All patterns are plotted on a logarithmic scale. A solid grey line represents the boundary between air and the dielectric environment. Solid grey lines are also used to indicate the critical angle window for the lossless dielectric half-spaces.

Three environments were investigated, two were lossless dielectric half-spaces with relative permittivities of 5 and 20, and the third was a heterogeneous environment with a stochastic distribution of the soil properties. The soil properties were: a sand fraction of 0.5, a clay fraction of 0.5, a bulk density of 2 g/cm^3, a sand particle density of 2.66 g/cm^3, and a volumetric water content range of 0.001–0.25. 50 different materials were created in the model to simulate this volumetric water content range.

Radiation patterns in the the three environments were calculated every 0.01 m from a distance of 0.10 m to 0.29 m.

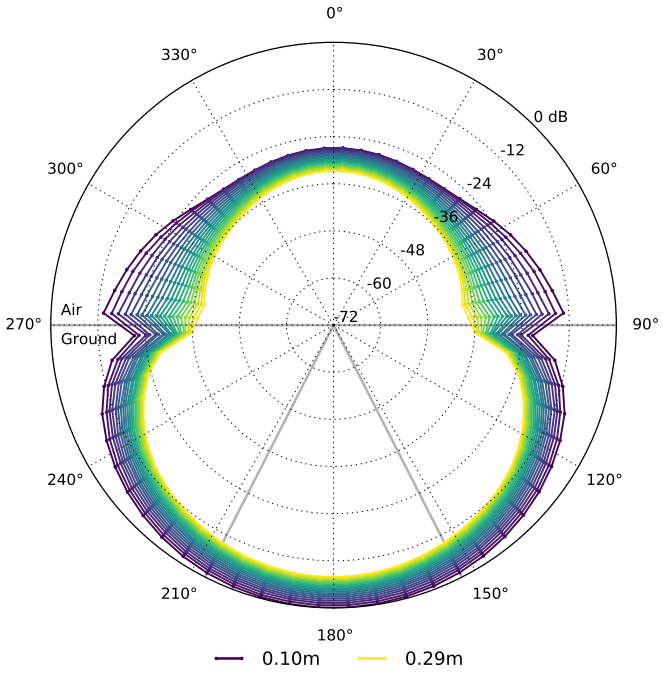

(a) E-plane

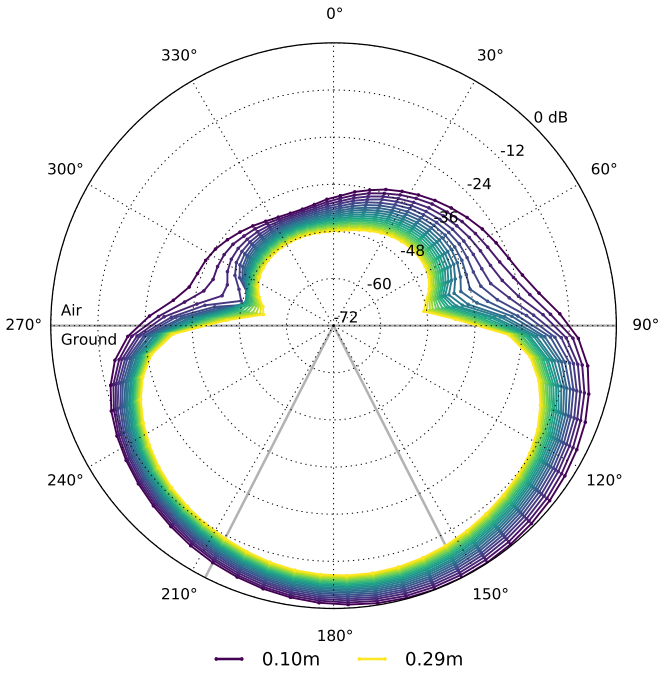

(b) H-plane

Fig. 3. Series of patterns from GSSI 1.5 GHz antenna model over a dielectric half-space of relative permittivity 5. Observation distances $0.10 - 0.29$ m at intervals of 0.01 m.

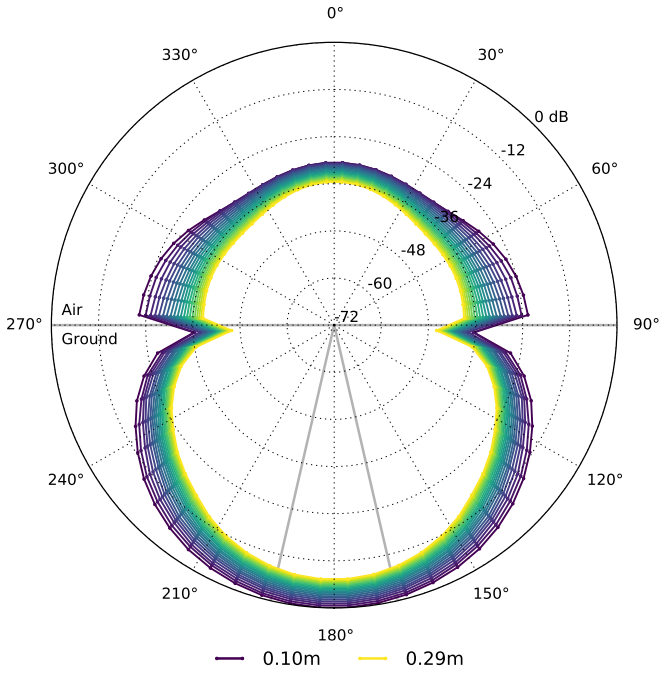

(a) E-plane

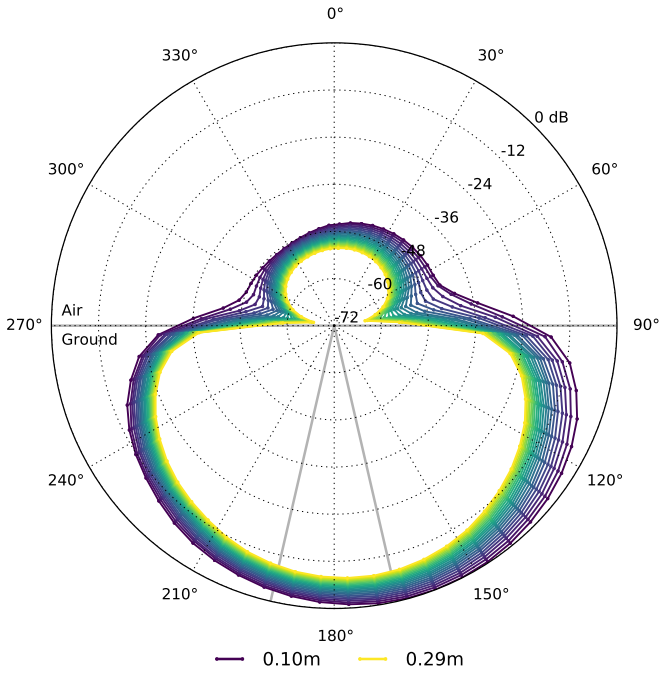

(b) H-plane

Fig. 4. Series of patterns from GSSI 1.5 GHz antenna model over a dielectric half-space of relative permittivity 20. Observation distances $0.10 - 0.29$ m at intervals of 0.01 m.

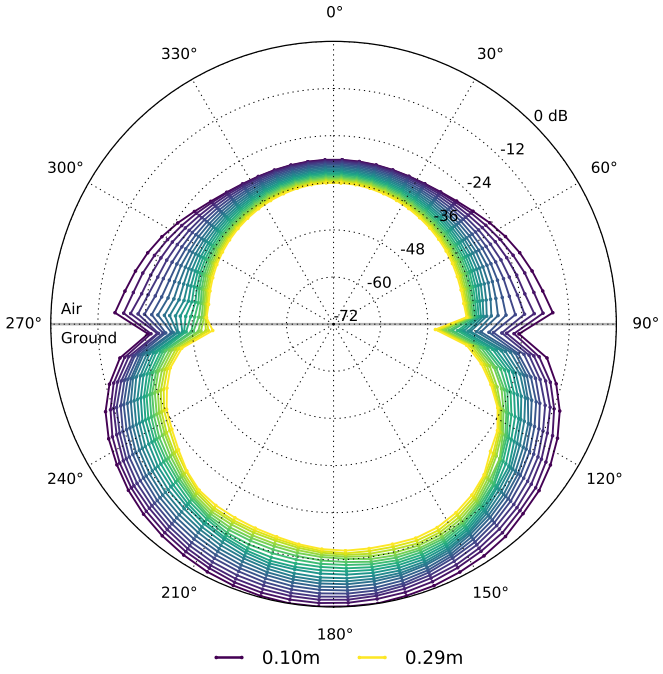

(a) E-plane

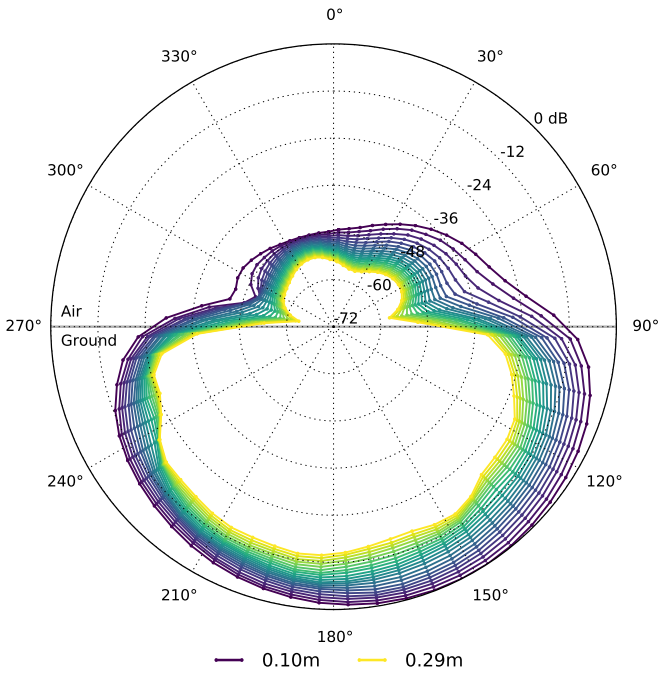

(b) H-plane

Fig. 5. Series of patterns from GSSI 1.5 GHz antenna model over a lossy, heterogeneous environment with static relative permittivities from 5–20. Observation distances $0.10 - 0.29\ m$ at intervals of $0.01\ m$.

The maximum distance was limited by the computational resources available at the time. Further models are planned when access to a high-performance computing (HPC) machine becomes available. In any case, the antenna is high-frequency and ground-coupled so most targets will be detected in the near-field of the antenna. Over a lossless dielectric of relative permittivity 5 the theoretical transition from near-field to far-field zones, (the Fraunhofer distance) based on Eq. (2), occurs at 0.0806 m. For a relative permittivity 20 the distance is 0.1611 m. Therefore, far-field behaviour (in theory) should be visible in both lossless dielectric environments.

$$R = \frac{2D^2}{\lambda}, \tag{2}$$

where D is the largest dimension of the antenna (0.060 m), and λ is the wavelength in the medium.

Figs. 3–4 present the principal E- and H-plane patterns in lossless dielectric environments of relative permittivity 5 and 20. As expected all of the patterns show a broad main lobe. Maximum power in the E-plane is directly under the antenna (180°). It can be observed that because the T_x and R_x elements of the antenna are offset from each another, the H-plane patterns are asymmetric about the vertical axis (0°,180°). Consequently, maximum power in the H-plane is offset towards the T_x element ($\approx 150°$). As the observation distance (r) increases from 0.01 m to 0.29 m the maximum power decreases following an exponential relationship (e^{-ar}), rather than a power relationship ($\frac{1}{r}, \frac{1}{r^2}, \frac{1}{r^3}...$) predicted by theory. In addition, the overall shape of the pattern begins to converge to a constant one, moving towards far-field behaviour, as the observation distance increases. However, the distance at which the far-field begins is clearly greater than that predicted by theory (the Fraunhofer distance). As the permittivity of the dielectric environment increases the main lobes in both E- and H-plane patterns become narrower. This occurs because the critical angle becomes smaller as the permittivity of the dielectric environment increases. Energy in the critical angle window mainly comes from the spherical wave in the ground, whereas energy beyond the critical angle window is associated with lateral waves.

Fig. 5 presents the principal E- and H-plane patterns in a lossy, heterogeneous environment with static relative permittivities from 5–20. There are several important differences between the half-space dielectric environments and the heterogeneous one (representative of a realistic soil). Firstly, because the heterogeneous environment is lossy, the difference in maximum power between observation distances of 0.01 m and 0.29 m is up to 20 dB, compared to up to 10 dB in the homogeneous dielectric half-space. Asymmetry is now present in the shape of both the E- and H-plane patterns because of the heterogeneous nature of the environment. The overall shapes of the E- and H-plane patterns are less smooth, and as the observation distance increases the shapes do not converge to constant ones as happened in the lossless dielectric environments. There are noticeable dips in gain in the main lobe of the H-plane pattern at around 130° and 245° at larger

observation distances. This is significant as the H-plane is the plane in which GPR surveys are usually performed.

IV. Conclusion

An advanced FDTD modelling toolset has been developed to allow a detailed model of a high-frequency GPR antenna to be investigated in lossless and lossy, heterogeneous environments. A stochastic distribution of soil properties (clay fraction, sand fraction, bulk density, sand particle density, and volumetric water fraction) was used to simulate a realistic soil (lossy, heterogeneous environment). Principal field patterns were used to analyse the behaviour of the antenna.

Simulations using the antenna model with lossless dielectric half-spaces provide a basic guide to how the antenna will perform in more realistic environments. However, important differences in the directivity (power and pattern shape) of the antenna were observed when the antenna model was used in the lossy, heterogeneous environment. Further research is required to investigate these phenomena at greater observation distances, in other soil environments, and with different stochastic distributions of soil properties.

References

[1] S. Millard, A. Shaari, and J. Bungey, "Field pattern characteristics of gpr antennas," *NDT and E International*, vol. 35, no. 7, pp. 473–482, 2002.

[2] G. Klysz, X. Ferrieres, J. Balayssac, and S. Laurens, "Simulation of direct wave propagation by numerical fdtd for a gpr coupled antenna," *NDT & E International*, vol. 39, no. 4, pp. 338–347, 2006.

[3] V. Pérez-Gracia, D. Di Capua, R. González-Drigo, and L. Pujades, "Laboratory characterization of a gpr antenna for high-resolution testing: Radiation pattern and vertical resolution," *NDT & E International*, vol. 42, no. 4, pp. 336–344, 2009.

[4] A. Annan, W. Waller, D. Strangway, J. Rossiter, J. Redman, and R. Watts, "The electromagnetic response of a low-loss, 2-layer, dielectric earth for horizontal electric dipole excitation," *Geophysics*, vol. 40, pp. 285–298, 1975.

[5] S. Arcone, "Numerical studies of the radiation patterns of resistively loaded dipoles," *Journal of Applied Geophysics*, vol. 33, pp. 39–52, 1995.

[6] C. Warren and A. Giannopoulos, "Experimental and modeled performance of a ground penetrating radar antenna in lossy dielectrics," *Selected Topics in Applied Earth Observations and Remote Sensing, IEEE Journal of*, 2015.

[7] S. Lambot, E. C. Slob, I. van den Bosch, B. Stockbroeckx, and M. Vanclooster, "Modeling of ground-penetrating radar for accurate characterization of subsurface electric properties," *Geoscience and Remote Sensing, IEEE Transactions on*, vol. 42, no. 11, pp. 2555–2568, 2004.

[8] S. Lambot, F. André, E. Slob, and H. Vereecken, "Effect of antenna-medium coupling in the analysis of ground-penetrating radar data," *Near Surface Geophysics*, vol. 10, no. 6, pp. 631–639, 2012.

[9] N. Diamanti and A. P. Annan, "Characterizing the energy distribution around gpr antennas," *Journal of Applied Geophysics*, vol. 99, pp. 83–90, 2013.

[10] A. Giannopoulos, "Modelling ground penetrating radar by gprmax," *Construction and building materials*, vol. 19, no. 10, pp. 755–762, 2005.

[11] L. Galagedara, J. Redman, G. Parkin, A. Annan, and A. Endres, "Numerical modeling of GPR to determine the direct ground wave sampling depth," *Vadose Zone Journal*, vol. 4, pp. 1096–1106, 2005.

[12] M. Jeannin, S. Garambois, C. Grégoire, and D. Jongmans, "Multiconfiguration GPR measurements for geometric fracture characterization in limestone cliffs (Alps)," *Geophysics*, vol. 71, p. B85, 2006.

[13] O. Lopera and N. Milisavljevic, "Prediction of the effects of soil and target properties on the antipersonnel landmine detection performance of ground-penetrating radar: A Colombian case study," *Journal of Applied Geophysics*, vol. 63, no. 1, pp. 13–23, 2007.

[14] F. Soldovieri, J. Hugenschmidt, R. Persico, and G. Leone, "A linear inverse scattering algorithm for realistic GPR applications," *Near Surface Geophysics*, vol. 5, no. 1, pp. 29–42, 2007.

[15] Elsevier. Scopus, the largest abstract and citation database of peer-reviewed literature. [Online]. Available: http://www.scopus.com

[16] C. Warren and A. Giannopoulos, "Creating FDTD models of commercial GPR antennas using Taguchi's optimisation method," *Geophysics*, vol. 76, no. 37, 2011.

[17] M. C. Dobson, F. T. Ulaby, M. T. Hallikainen, and M. A. El-Rayes, "Microwave dielectric behavior of wet soil-part ii: Dielectric mixing models," *Geoscience and Remote Sensing, IEEE Transactions on*, no. 1, pp. 35–46, 1985.

[18] I. Giannakis and A. Giannopoulos, "A novel piecewise linear recursive convolution approach for dispersive media using the finite-difference time-domain method," *Antennas and Propagation, IEEE Transactions on*, 2014.